EPS-0473
Submitted to Pa 17 and Pl 2

Elastic Photoproduction of ρ^0 Mesons at HERA

H1 Collaboration

Abstract

The cross section for the elastic photoproduction of ρ^0 mesons is measured with the H1 detector at HERA at two average photon-proton center-of-mass energies $\langle W_{\gamma p}\rangle$ of 55 and 187 GeV. The low energy point was measured by directly observing the ρ^0 decay giving a $\sigma(\gamma p \rightarrow \rho^0 p)$ of $11.4 \pm 0.8\,(stat.) \pm 2.6\,(syst.)\,\mu$b. The slope parameter of the differential distribution dN/dt was found to be $9.4 \pm 1.4(stat.) \pm 0.7(syst.)$ GeV^{-2} and the ρ^0 decay angular distribution was found to be consistent with s-channel helicity conservation. The high energy measurement was made by inference from the lower part of the inclusive photon diffractive invariant mass spectrum. A value for $\sigma(\gamma p \rightarrow \rho^0 p)$ of $13.9 \pm 0.9(stat.) \pm 2.2(syst.)\mu$b was found.

1 Introduction

The photon, exhibiting both point-like and hadronic behavior, has a rich structure that is still not well explored. New opportunities for studying photon interactions are opened by the HERA electron-proton collider. The virtual photons produced by HERA's electron beam extend the energy range for photoproduction processes by more than one order of magnitude, up to the equivalent of tens of TeV in fixed target experiments, providing a a large kinematic range for studying the properties of the photon. The H1 and ZEUS collaborations have recently begun to explore this domain with measurements of the total γp cross section [1, 2] and vector meson production [2, 3].

In this paper we report the H1 results of the elastic ρ^0 photoproduction cross section at an average total energy, $\langle W_{\gamma p}\rangle$, in the γp center-of-mass system (cms), of 55 and 187 GeV. For the low energy measurement the associated differential distribution in t, the square of the four-momentum transfer, and the decay angular distribution of the ρ^0 are also presented.

At lower energies the photon is known to exhibit behavior resembling that of a hadron. In particular, the reaction

$$\gamma + p \to \rho^0 + p \tag{1}$$

at cms energies of 10-20 GeV behaves much as elastic scattering of hadrons: the cross section grows slowly with cms energy, the dependence on t is close to exponential, and s-channel helicity conservation holds (the ρ^0 retains the helicity of the photon). This is interpreted in the Vector Meson Dominance (VMD) model as the fluctuation of the photon into a virtual ρ^0 meson, with subsequent elastic scattering of the ρ^0 on the proton. Regge theory [4] inspired models have been used to describe successfully the energy variation of the total cross section, with the pomeron term dominating at high energies [5]. Mini-jet models may combine a soft VMD component with perturbatively calculable components to arrive at a total γp cross section. The $\gamma p \to \rho^0 p$ cross section then may be completely determined by the parameters used to fit the total γp cross section [6]. In these models, both the total cross section and the elastic cross section at high energies are sensitive to the small-x behavior of the parton densities in the photon. Thus studies of reaction (1) at HERA energies help to constrain such models, as well as to clarify the nature of the pomeron. It is important to an eventual understanding of the photon to explore these interactions thoroughly in the HERA energy regime.

Almost-real photons, radiated at small angles by HERA's electron beam (26.7 GeV in 1993 and 27.6 GeV in 1994), can interact with the 820 GeV protons at very high energies in the γp cms. In the VMD model, one expects strong production of the vector meson series $\rho^0, \omega, \phi, J/\psi, \ldots$ along with other hadronic production. Elastic $\rho^0 p$ interactions are characterized by a low-$|t|$ scattering of the virtual ρ^0 meson and the proton, leading to a ρ^0 at low p_t relative to the HERA beam axis. The ρ^0 subsequently decays into a lone $\pi^+\pi^-$ pair.

The kinematical variables are defined as follows:

$$\begin{aligned} Q^2 &= -(k-k')^2 = q^2 \\ t &= (q-v)^2 = (P-P')^2 \end{aligned}$$

$$
\begin{aligned}
y &= \frac{q \cdot P}{k \cdot P} \\
x &= \frac{Q^2}{2P \cdot q} \\
s &= (P+k)^2 \\
W_{\gamma p} &= \sqrt{ys}
\end{aligned}
$$

where $k(k')$ stands for the incoming (scattered) electron, $P(P')$ for the incoming (scattered) proton, q for the photon and v for the vector meson four vector. In H1 forward (backward) refers to the proton (electron) beam direction.

Over the wide range of $W_{\gamma p}$ accessible at HERA (from ≈ 1.2 GeV up to ≈ 300 GeV) two distinct experimental domains are apparent; one at low values of $W_{\gamma p}$ (from ≈ 20 GeV up to ≈ 100 GeV) where the scattered electron is not detected by H1 but where the ρ^0 decay products are visible in the central tracking detectors (CTD), and the other at high values of $W_{\gamma p}$ (from ≈ 165 GeV up to ≈ 213 GeV) where the scattered electron is tagged but where the ρ^0 decay products lie outside of the acceptance range of the CTD. In both the scattered proton is not detected. Since each domain requires rather different experimental techniques, two independent analyses are reported in this paper.

For the untagged, low $W_{\gamma p}$, analysis, $W_{\gamma p}$ and t are reconstructed from the products of the ρ^0 decay under the assumptions of an elastic interaction and $Q^2 = 0$ GeV^2 [1]. For the tagged sample, $W_{\gamma p}$ is reconstructed from the electron energy and detector resolution is such that no precise measurement of t is possible.

In our analysis we ignored the lepton beam polarization and we found that the longitudinal (helicity 0) contribution to the γp cross section was small. In this case the flux for transverse virtual photons is given by the Weizsäcker-Williams approximation

$$\frac{d^2\mathcal{L}_T}{dy\, dQ^2} \approx \frac{\alpha}{2\pi}\frac{1}{Q^2}\left(\frac{[1+(1-y)^2]}{y} - \frac{2m^2 y}{Q^2}\right).$$

In reference [8] the dependence of the photon flux on the lepton beam mass terms are derived by using the lepton-nucleon tensor to define the matrix element at the γp vertex.

The resulting ep cross section has the general form

$$\frac{d^2\sigma(ep)}{dy\, dQ^2} \approx \frac{\alpha}{2\pi}\frac{1}{Q^2}\left(\frac{[1+(1-y)^2]}{y} - \frac{2m^2 y}{Q^2}\right)\sigma(\gamma p \to \rho^0 p)(y, Q^2). \tag{2}$$

We use the flux factor in front of $\sigma(\gamma p \to \rho^0 p)(y, Q^2)$ to generate the Monte Carlo (MC) weights in our MC for ρ^0 production.

2 The H1 Detector

A complete description of the detector being available elsewhere [9], we only briefly describe here the parts of the detector relevant to this analysis. The H1 Central Tracking

[1]The minimum value of Q^2 at the largest value of $W_{\gamma p}$ reached in this analysis is 2.3×10^{-9} GeV^2, which is effectively zero for our purposes.

Detector (CTD) consists of two concentric drift chambers, Central Jet Chambers 1 and 2 (CJC1 and CJC2), and two thin proportional chambers, the Central Inner and Central Outer Proportional Chambers (CIP and COP), located at the inner radii of CJC1 and CJC2, respectively. The entire CTD system functions within a 1.13 T solenoidal magnetic field, parallel to the proton beam axis (polar angle $\theta = 0°$). The CJC's provide tracking information in the range of $-1.5 < \eta < 1.5$ in pseudorapidity, with $\eta = -\ln(\tan(\theta/2))$, and a fast drift chamber trigger (DCRϕ) for the low $W_{\gamma p}$ analysis. Hit pads in the two active layers in each of CIP and COP are used in the trigger to veto events with large multiplicities.

The CTD is surrounded by a liquid Argon (LAr) calorimeter that covers the angular range ($-1.5 < \eta < 3.3$). It is used both as a veto of inelastic events and to optimize the hadronic final state in the high $W_{\gamma p}$ analysis.

The main detector is surrounded by the instrumented iron which provides tracking and calorimetry information. It is used in this analysis to veto cosmic muon events.

In the forward region, two detectors are used to veto events that have forward activity; the forward muon detector (FMD) and the proton remnant tagger (PRT). They are used in this analysis to tag hadrons produced at large values of pseudorapidity ($5.0 < \eta < 7.5$) by detecting secondary particles issued from collisions with the beam pipe or adjacent material.

The backward region is covered in the range $-3.4 < \eta < -1.5$ by a lead scintillator calorimeter (BEMC) used to reconstruct the hadronic final state in the the high $W_{\gamma p}$ analysis and in the range $-3.0 < \eta < -1.5$ by the backward proportional chamber (BPC) used to reject beam-gas background. Behind the BEMC are located the Time of Flight (ToF) scintillator walls covering a pseudorapidity range of $-3.5 < \eta < -2.0$. They are used to reject background upstream proton interactions and as a trigger in the high $W_{\gamma p}$ analysis.

The luminosity system, measuring the reaction $ep \to e\gamma p$, consists of two TlCl/TlBr crystal calorimeters. The electron tagger is located at $z = -33$ m and the photon detector at $z = -103$ m. The electron tagger is also used in the trigger of the high $W_{\gamma p}$ analysis.

3 Monte Carlo

Two Monte Carlo generators were used in this analysis, PYTHIA [13] and PHOJET [14]. Five MC photoproduction mechanisms are distinguished: elastic (EL) which describe $ep \to epV^0$, single photon diffractive dissociation (GD) in which the photon dissociates, single proton diffractive dissociation (PD) in which the proton dissociates, double diffractive dissociation (DD) in which both dissociate, and non-diffractive (ND). This last class includes the description of the $ep \to X$ reaction not belonging to the previous classes.

Both MC's have similar inputs for the EL channel. Events are generated with a t-dependence of e^{bt} where $b \approx 11$ GeV^{-2}, and a a decay angular distribution proportional to $\sin^2\theta^*$ as expected from a transversely polarized photon (helicity ± 1).

The other channels are described in more detail in [24]

4 The Low $W_{\gamma p}$ Analysis

The data for this analysis were taken in 1993 when HERA operated with 90 bunches of 820 GeV protons and 94 bunches of 26.7 GeV electrons with 84 colliding bunch pairs. A small number of non-colliding electron and proton bunches, called "pilot" bunches, were included in order to estimate the beam-gas background, with current ratios relative to the "colliding current" of 1/14.39 for p-pilot and 1/8.46 for e-pilot. For consistent performance, we limit our data sample (19.75nb^{-1}) to the largest continuous segment of runs containing 100% stable and uniform central tracker conditions.

The more favorable of the standard H1 triggers, which should be able to distinguish the soft, low multiplicity final state in a high background level, utilize the drift chamber trigger components (DCRϕ) and find tracks by a fast pattern matching of hits. Unfortunately, their efficiency threshold as a function of transverse momentum p_t is between 0.4 and 0.5 GeV/c, where the spectrum of the decay products of the elastic ρ^0 is already falling. In such conditions, the best combination of trigger signals turns out to require one and only one track pattern identified by the DCRϕ triggers, hence relying on their inefficiencies for the detection of both tracks of the ρ^0 decays but rejecting all the low p_t background. In addition, the central proportional chambers provide trigger signals [10] requiring a single z-vertex candidate in each event and a veto on events with excessive activity in the backward portion of the inner detectors. Finally, the conditions of the LAr's veto on Inner Forward (IF) energy and the ToF's timing are also required.

Because our analysis uses only two prong events, the selection procedure is particularly sensitive to errors in event multiplicity. We have observed differences between the data and MC track reconstruction efficiencies, leading to a discrepancy in the determination of event multiplicity. Therefore, a visual scan early in the analysis was found to be necessary to determine data and MC reconstruction efficiencies accurately.

140×10^3 events satisfied the trigger. This number was reduced by a computer filter essentially independent of track reconstruction quality thus eliminating only obvious non two prong events.

The reduced sample of $\approx 47 \times 10^3$ events was then scanned visually with the H1 event display program. We required two opposite sign track patterns pointing to a common vertex and which reached at least CJC2 ($r \gtrsim 43$ cm). Only digitized hit information from the CJC detectors was used in the scan. Obvious cosmic events with tracks in the instrumented iron were removed. A total of 12,200 valid two prong opposite-sign events passed the scan including 623 from the p-pilot bunch crossings, 13 from the e-pilot bunch crossings, and 50 from the empty bunch crossings.

The events were then reconstructed using the standard H1 reconstruction program. The data and MC samples produce different reconstruction efficiencies of 0.8430 ± 0.0034 and 0.8807 ± 0.0022 respectively. The ratio of the data to MC efficiencies is used as a correction factor to account for differences in track fitting (C in Eq. 4).

The reconstruction of the kinematics can be done accurately from the ρ^0 alone, as shown in Figs. 1a and 1b where the generated $W_{\gamma p}$ and t variables respectively, are compared to the corresponding computed values.

The final set of cuts kinematically reduces the number of background events. Each event is required to have:

- $W_{\gamma p} > 40$ GeV, cutting most of the p-gas present in data.
- Total energy in the LAr inner forward wheel: $E_{IF} < 0.4$ GeV, suppresses events containing hadronic debris in the forward (proton) direction.
- Track-pair $p_t^2 < 0.5$ (GeV$/c)^2$, reduces the amount of dissociative events.
- The high p_t track in an event: $p_t > 0.5$ GeV$/c$ and the low p_t track in an event $p_t <$ 0.4 GeV$/c$, matches the region of flat efficiency for the elastic ρ^0 trigger.
- $m_{\pi\pi} \in [0.370, 1.167]$ GeV$/c^2$, to match the mass range generated for elastic ρ^0 events in the MC.

A total of 358 colliding bunch events and 0 pilot or empty bunch events survive all cuts.

We measured the efficiency of this trigger using an independent sample of events triggered on the electron tagger. Although the electron detected is not the one from the reaction $ep \rightarrow ep\rho^0$, once the same selection procedure and cuts are applied as on the data, we are left with a data set comparable to that of the final rho sample. It was not possible to find a sample of events which was simultaneously independent and unbiased with respect to all the components of the trigger used. Therefore we determined separately the efficiencies of 3 components (z-vertex; CTD dependent triggers and ToF component; LAr veto) from sub-samples of electron tagger (e-tag) events. The final trigger efficiency was experimentally obtained from the separate measured components by multiplying the results together and was found to be $\epsilon_{trig} = 0.21 \pm 0.04$. The error is purely due to the low statistics available.

The five MC processes described above were simulated within PYTHIA are with the following combination of cross section ratios, as extrapolated from fits of low energy data [15]:

$$\sigma_{EL} : \sigma_{GD} : \sigma_{PD} : \sigma_{DD} : \sigma_{ND} = 1 : 0.79 : 0.71 : 0.33 : 5.0\,. \tag{3}$$

Only the elastic, the photon diffractive and the proton diffractive components contribute significantly to the final sample; the others are almost entirely excluded by the selection process. The sensitivity of the result to variations in the ratios is discussed below. The acceptance, A_i, for each process is determined with the standard H1 simulation and reconstruction programs. These are entered into the calculation of the elastic cross section:

$$\sigma(\gamma p \rightarrow \rho^0 p) = \frac{N_{observed} \times 0.88}{[A_{EL} + \sum_{i=GD,PD,DD,ND} R_{i:EL} A_i]\, \mathcal{L}_{ep}\, f\, \epsilon_{trig}\, C} \tag{4}$$

where ϵ_{trig} is the trigger efficiency and C, a correction factor, accounts for the different track reconstruction efficiencies for the data and MC events (see section 4.1) and $f =$ 0.25311 is the flux factor integrated over the kinematic range by IJRAY. The factor of 0.88 holds for the fraction of ρ^0's in the elastic sample at the generator level.

5 The High $W_{\gamma p}$ Analysis

The data for this measurement were collected during a short dedicated run during the 1994 data taking period with a vertex shifted forward of its nominal position by ≈ 70 cm.

With this vertex position the acceptance for particles traveling backwards at small angles to the beam pipe is enhanced. The HERA machine was operated with 153 colliding bunches of 27.6 GeV positrons and 820 GeV protons with in addition, 17 proton and 15 positron pilot bunches. The data taken correspond to a total integrated luminosity of 23.8 nb^{-1}.

Photoproduction events were triggered by the coincidence of signal in the electron tagger ($E'_e > 4$ GeV) and a signal in the ToF system coming from the time interval expected for ep interactions.

The main source of background in the triggered sample was found to be positron beam interactions with residual gas or with materials inside the beam pipe. This background was reduced by requiring at least one BPC hit and an energy deposition greater than 0.5 GeV in the BEMC or LAr calorimeters. The measurement was further restricted to the kinematic range $0.3 < y < 0.5$ where the electron tagger acceptance is good.

Diffractive events (mainly GD and EL) were selected by requiring no activity above threshold in the forward detectors (FMD and PRT) and the pseudorapidity of the most forward energy deposit in the LAr calorimeter (η_{max}) to be less than 3.

The four vector (E_h, Px_h, Py_h, Pz_h) of the hadronic final state was determined by combining calorimeter and tracking information. The invariant mass of the hadronic final state excluding the proton, M_X was then calculated as follows:

$$M_X = \sqrt{(E_h + Pz_h) \cdot 2 \cdot E_e \cdot y}, \tag{5}$$

where E_e is the positron beam momentum and y is reconstructed from the final state positron. This method resulted in a resolution σ_{M_X} of $\approx 30\%$ even though a significant proportion of the hadronic energy is not detected in the backward region.

A sample of events (called here after 'the low mass sample') where elastic (ρ^0, ω, ϕ) production dominates was selected by requiring $M_X < 1.26$ GeV and $\eta_{max} < -1.5$. Plots of the reconstructed mass spectrum for the diffractive and low mass samples are shown in figure 2. It should be noted that σ_{M_X} is much greater than the width of the ρ^0 decay, making it impossible with this analysis to determine the line shape.

Background in the low mass sample sample was found to arise from three dominant sources: positron beam induced background; migrations from high mass photon diffraction due to imperfect resolution in M_X and proton diffraction where none of the proton fragments were detected.

The positron beam induced background was estimated using pilot bunch events and found to contribute $\approx 20 \pm 5\%$ to the observed signal.

The MC generators (PYTHIA and PHOJET) were used to estimate the fraction of GD and PD background. The GD cross section was constrained by comparison of the number of observed events in data and MC in the photon diffractive sample for $M_X > 1.26$ GeV. The PD cross section was constrained by making an event selection that required some energy to be detected in the forward part of the LAr calorimeter or in one of the forward detectors. Non-diffractive events were suppressed by requiring a central gap in the LAr calorimeter. The hadronic final state was reconstructed using tracks and energy depositions detected more backward of the central gap. Placing a cut of $M_X < 1.26$ GeV resulted in a relatively pure sample of PD events from which the MC cross section could be compared. The GD and PD background fractions were estimated to be 10% and 8% respectively and subtracted from the sample.

The acceptance (including the trigger acceptance) for the low mass sample was determined using the two MC generators. Both gave similar values of about 50 % for detection of hadronic final state and about 60 % for detection of the positron. For the results and plots shown the average of the two MCs was used.

6 Results

6.1 The Cross Section

In the low $W_{\gamma p}$ analysis the final MC cross section sample indicates that the observed ρ^0 events come predominately from elastic (76%), photon diffractive (9%) and proton diffractive (13%) production, with doubly diffractive contributing a small fraction (2%) and non-diffractive entirely absent. Figure 3 shows the dipion mass spectra of the accepted data and MC events. The MC mass shape, containing a skewed mass distribution for the elastic ρ^0 events, matches the shape of the data histogram well.

Combining the observed events from data, acceptance from MC (139.8 events/μb), trigger efficiency (0.21 ± 0.04), and the reconstruction correction factor (0.957 ± 0.004), the cross section for elastic ρ^0 photoproduction is measured to be (PRELIMINARY):

$$\sigma(\gamma p \to \rho^0 p) \quad = \quad 11.4 \pm 0.8\ (stat.) \pm 2.8\ (syst.) \pm 0.6\ (lumi.)\ \mu\text{b}$$

The cross section is taken over the range in the γp center of mass energy between 40 and 90 GeV, with a mean of $\langle W_{\gamma p} \rangle = 55$ GeV.

The primary source of systematic error for the cross section measurement comes from the determination of the trigger efficiency (20 %). Model uncertainty and theoretical prejudices allow the cross sections to vary by 10 % [16]. We conservatively estimate model dependence by varying the assumed ratio of the inelastic to elastic cross sections, $R_{inelastic}$, by 20 % and the background MC acceptances by 50 %. The resulting calculations of $\sigma(\gamma p \to \rho^0 p)$ vary by 11.1 %. The systematic error associated with the scan is taken to be the statistical spread on scanning yield (6.5 %). Track fitting systematics are estimated by taking the difference between the data and MC rates for the successful reconstruction of a track pair (4.3%, see section 4.1). Finally, the statistical error on MC acceptance is 3.1%. All sources are combined in quadrature for a total systematic error of 24 %.

In the high $W_{\gamma p}$ analysis the low mass cross section was converted to an elastic cross section with estimates of the inelastic contribution for $2M_\pi < M_X < 1.26$ GeV taken from experiments at lower energy [17] and to a ρ^0 cross section using the prediction of [18] for the contributions from ω^0 and ϕ^0 production in the elastic peak. The corrections amounted to a total reduction in the cross section of 22% (7% inelastic, 9% ω^0 and 6% ϕ^0). which then became (PRELIMINARY):

$$\sigma(\gamma p \to \rho p) = 13.9 \pm 0.9(stat.) \pm 2.1(syst.) \pm 0.7(lumi.)\ \mu\text{b}. \tag{6}$$

A breakdown of the systematic errors is shown in the table 1.

Source	Method	Error
MC acceptance	PYTHIA-PHOJET difference, statistics	5 %
BEMC scale	vary BEMC scale by 20%	4 %
t dependence	vary t slope by 30%	3 %
elastic contribution	vary ω^0 and ϕ^0 contributions by 50%	7 %
GD contribution	vary MC prediction by 50%	7 %
PD contribution	vary MC prediction by 50%	4 %
e-gas background	vary e-gas contribution by 25%	5 %
e-tagger acceptance	positron beam optics	5 %
Total systematic		15 %

Table 1: Sources of systematic errors for the elastic ρ^0 cross section measurement at $\langle W_{\gamma p}\rangle = 187$ GeV.

The total cross sections of H1 and ZEUS [1, 2] have already placed constraints on mini-jet model parameters and parton density distributions of the photon. With a lower limit of 4 $(\text{GeV}/c)^2$ on the integration over p_t^2 and a parton density function in the photon that is not too large (*e.g.*, DG from [19]) the mini-jet approach can describe the rise of the total cross section from a few GeV to HERA energies. The same parameters then also give a satisfactory fit to the elastic ρ^0 photoproduction cross section over the same range of $\sqrt{s}$ [6]. Similarly, mini-jet models with very steep parton densities in the photon (e.g., LAC1 [20]) do not give the correct rise of the total cross section and also do not fit the elastic ρ^0 results. Fig. 4 compares this measurement with previous determinations of the elastic ρ^0 cross section [2, 3, 21] and theoretical predictions based on the additive quark model and VMD [5] (solid curve) and mini-jets [6] with DG and $p_t^2 = 4$ $(\text{GeV}/c)^2$ (dot-dashed curve) and with LAC1 and $p_t^2 = 4$ $(\text{GeV}/c)^2$ (dashed curve).

6.2 The dN/dt Distribution

Diffraction is characterized by a low-momentum transfer between the vector meson and the proton, resulting in a steeply falling distribution in t. Elastic events exhibit a steeper distribution than inelastic diffractive events. This is quantified by the slope parameter, b, determined by fitting the t distribution to the function $a\,e^{bt}$.

A modified analysis is used in the determination of the slope parameter, b. Since the cuts in track p_t, required for a flat trigger acceptance in the cross section measurement, severely distort the distribution and reduce the size of the event sample, we eliminate the $p_t^{high/low}$ cut from this part of the analysis. In order to model the trigger's p_t effects in the MC, we replace the cut with a requirement that the MC trigger be set. Consequently, we limit our analysis to a study of the differential distribution, dN/dt, not the absolute magnitude.

Before fitting, we subtract background contributions from the data and MC t distributions and then correct for losses due to acceptance. Since this set of cuts does yield two p-pilot events in the final data sample, these events are scaled up in proportion to the beam currents (see section 2.1) and then subtracted from data. A fourth-order polynomial fit to the inelastic MC distribution is taken as an estimate of the inelastic background and subtracted from the data. A fourth-order polynomial fit to the elastic MC acceptance distribution is then applied to produce the corrected distribution in t. The exponential fit of the final data distribution (see Fig. 5) gives a slope parameter of (PRELIMINARY):

$$b = 9.4 \pm 1.4 \ (stat.) \pm 0.7 \ (syst.) \ \mathrm{GeV}^{-2}$$

The same inelastic subtraction and acceptance correction procedures are applied to the combined MC sample. The exponential fit results in a slope parameter that matches to within 6.9% the value fit for the generator-level elastic ρ^0 distribution ($b = 10.9 \pm 0.2$). This difference is taken to be a systematic error. The error from using the $\pm 1\sigma$ extremes on the fit to the elastic acceptance in t, or from a 20% shift in $R_{inelastic}$ is negligible.

The measurement of b is compared to previous determinations in Figure 7. The recent ZEUS measurement [3] is shown along with lower energy data as compiled by Aston [22]. The ZEUS and H1 results together are consistent with a continued shrinkage of the elastic peak.

6.3 Angular Distribution of the ρ^0 Decay

In generating our MC sample, we have assumed an unpolarized proton beam, an electron beam with no spin longitudinal polarization, and that the amplitudes for $\gamma p \to \rho^0 p$ obey s-channel helicity conservation and natural parity exchange. Longitudinal lepton beam polarization effects are small at low Q^2 [7, 23]. Transverse lepton beam polarization effects, important at very low Q^2, are measurable only if the scattered electron is observed. Since we do not observe the scattered electron in the elastically produced ρ^0 meson events, we are justified in ignoring these azimuthal dependencies and can integrate over the azimuthal dependence on beam polarization. Following the formalism in Bauer, *et al.*, [18] we study the angular distribution of the π^- momentum vector arising from the decay of the ρ^0 in the cms. For a transversely polarized virtual photon, the normalized angular distribution of the π^- relative to the direction of the ρ^0 is:

$$W(\theta^*) = \frac{3}{4}\left[(3r_{00}^{04} - 1)\cos^2\theta^* + (1 - r_{00}^{04})\right]. \tag{7}$$

We apply to the $dN/d(\cos\theta^*)$ distribution the same selection, subtraction, and correction procedures used for the dN/dt analysis. The fit of the final distribution (Figure 6) leads to a value of (PRELIMINARY) $r_{00}^{04} = -0.041 \pm 0.048 \ (stat.) \pm 0.013 \ (syst.)$. The same procedure applied to the MC also gives a value compatible with $r_{00}^{04} = 0$, as assumed in the MC. The systematic error (32%) is calculated by varying $R_{inelastic}$ by 20%.

7 Conclusion

With the H1 detector, we have measured the cross section for the elastic photoproduction of ρ^0 mesons and find $\sigma(\gamma p \to \rho^0 p) = 11.4 \pm 0.8 \ (stat.) \pm 2.6 \ (syst.) \ \mu\mathrm{b}$ at $\langle W_{\gamma p}\rangle = 55$ GeV and $\sigma(\gamma p \to \rho^0 p) = 13.9 \pm 0.9\ (stat.) \pm 2.2\ (syst.)\ \mu$b at $\langle W_{\gamma p} \rangle = 187$ GeV. At the former $W_{\gamma p}$, the slope parameter of the distribution in t is $9.4 \pm 1.4\ (stat.) \pm 0.7\ (syst.)$ GeV^{-2}, and the decay angular distribution is consistent with a pure $\sin^2\theta$ distribution. We thus verify the extension to HERA energies of the properties found at lower energies for elastic photoproduction of the ρ^0 meson, namely a slow rise of the cross section with $W_{\gamma p}$, a steep forward distribution of the produced ρ^0 mesons, and a decay angular distribution that is consistent with s-channel helicity conservation.

References

[1] H1 Collab., T. Ahmed et al., Phys. Lett. B299 (1993) 374.

[2] ZEUS Collab., M. Derrick et al., Z. Phys. C63 (1994) 391.

[3] ZEUS Collab., M. Derrick et al., ICHEP94 Ref. 0688, Glasgow (1994).

[4] P. D. B. Collins, An Introduction to Regge Theory and High Energy Physics (Cambridge U. P., Cambridge, 2977).

[5] G. A. Schuler and T. Sjöstrand, Nucl. Phys. B407 (1993) 539.

[6] G. A. Schuler and J. Terron, Proc. HERA Workshop, Editors. W. Buchmüller and G. Ingelman, Hamburg (1992) Vol. 1, 599.

[7] K. Schilling and G. Wolf, Nucl. Phys. B61 (1973) 381.

[8] B. D. Burow, A Measurement of the Total Photon-Proton Cross Section in the Center of Mass Energy Range 167 to 194 GeV, Ph. D. Thesis, Dept. of Physics, University of Toronto (1994).

[9] H1 Collab., I. Abt et al., DESY preprint 93-103 (1993).

[10] S. Eichenberger et al., Nucl. Instr. and Meth. A323 (1992) 532.

[11] G. A. Schuler and T. Sjöstrand, CERN preprint TH. 7193/94 (1994).

[12] I. Abt, UCD/IIRPA preprint 93-240 (1993).

[13] T. Sjöstrand, Comp. Phys. Comm. 39 (1986) 347;
T. Sjöstrand and M. Bengtsson, Comp. Phys. Comm. 43 (1987) 367;
T. Sjöstrand and M. Bengtsson, Comp. Phys. Comm. 46 (1987) 43.

[14] R. Engel, Proceedings of the XXIXth Rencontre de Moriond (1994) 321.

[15] G. A. Schuler and T. Sjöstrand, Phys. Lett. B300 (1993) 169.

[16] T. Sjöstrand, private communication.

[17] T.J. Chapin et al., Phys. Rev. D31 (1984) 17.

[18] T. H. Bauer, F. M. Pipkin, R. D. Spital, and D. R. Yennie, Rev. Mod. Phys. 50 (1978) 261.

[19] M. Drees and K. Grassi, Z. Phys. C28 (1985) 451.

[20] H. Abramowicz, K. Charchula, and A. Levy, Phys. Lett. B269 (1991) 458.

[21] HERA and COMPAS Groups, CERN-HERA 87-01 (1987) 46.

[22] D. Aston et al., Nucl. Phys. B209 (1982) 56;
Y. Eisenberg et al., Phys. Rev. D5 (1972) 15;
G. Gladding et al., Phys. Rev. D8 (1973) 3721;
G. McClellon et al., Phys. Rev. Lett. 22 (1969) 374;
C. Berger et al., Phys. Lett. B39 (1972) 659.

[23] B. Dieterle, Il Nuovo Cimento 11A (1972) 523.

[24] Same conference EPS-0474

[25] A. Donnachie, P. V. Landshoff, Phys. Lett. B296 (1992) 227.

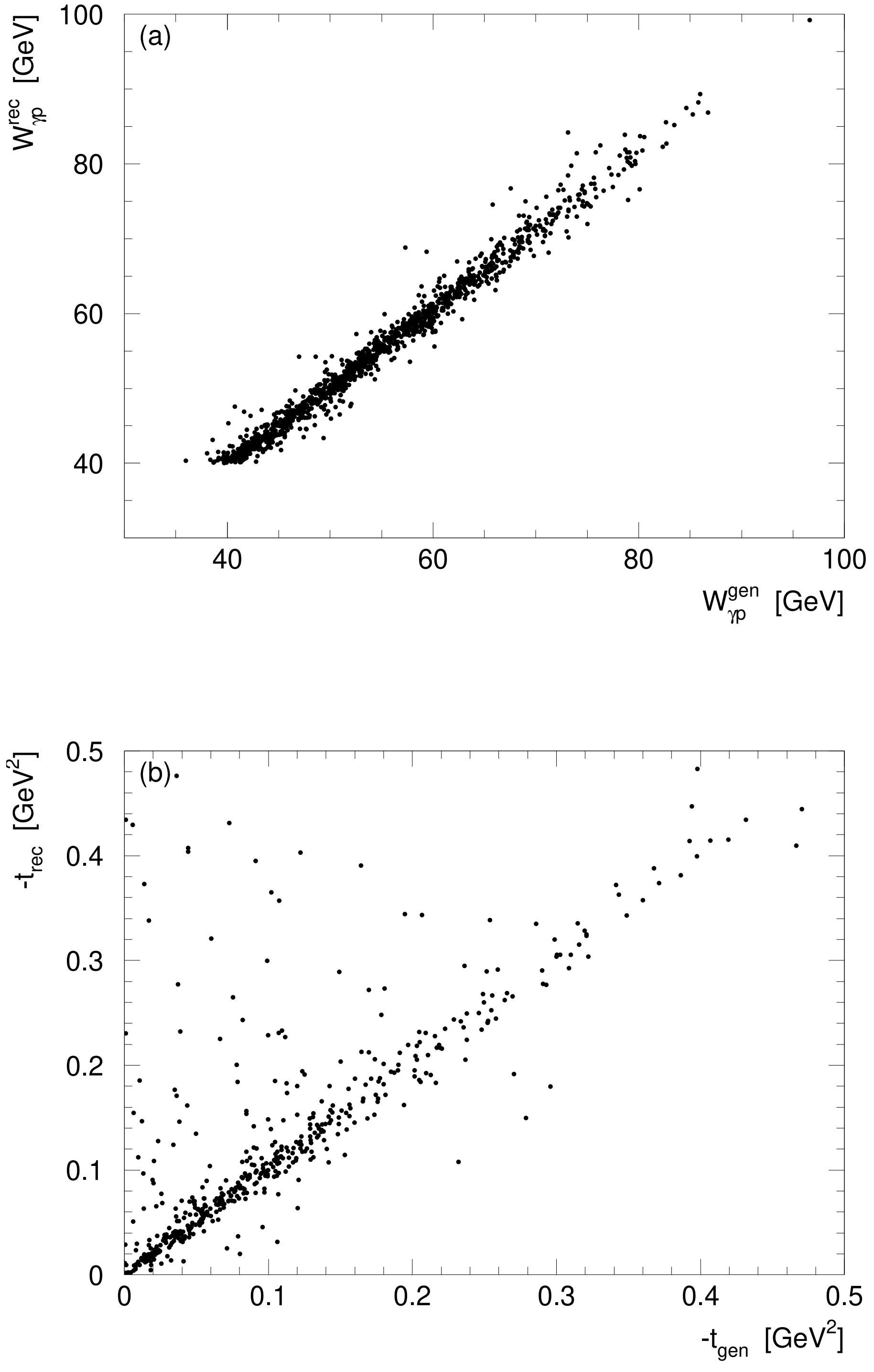

Figure 1: (a) MC reconstructed versus generated $W_{\gamma p}$; (b) MC reconstructed versus generated t for the low $W_{\gamma p}$ analysis.

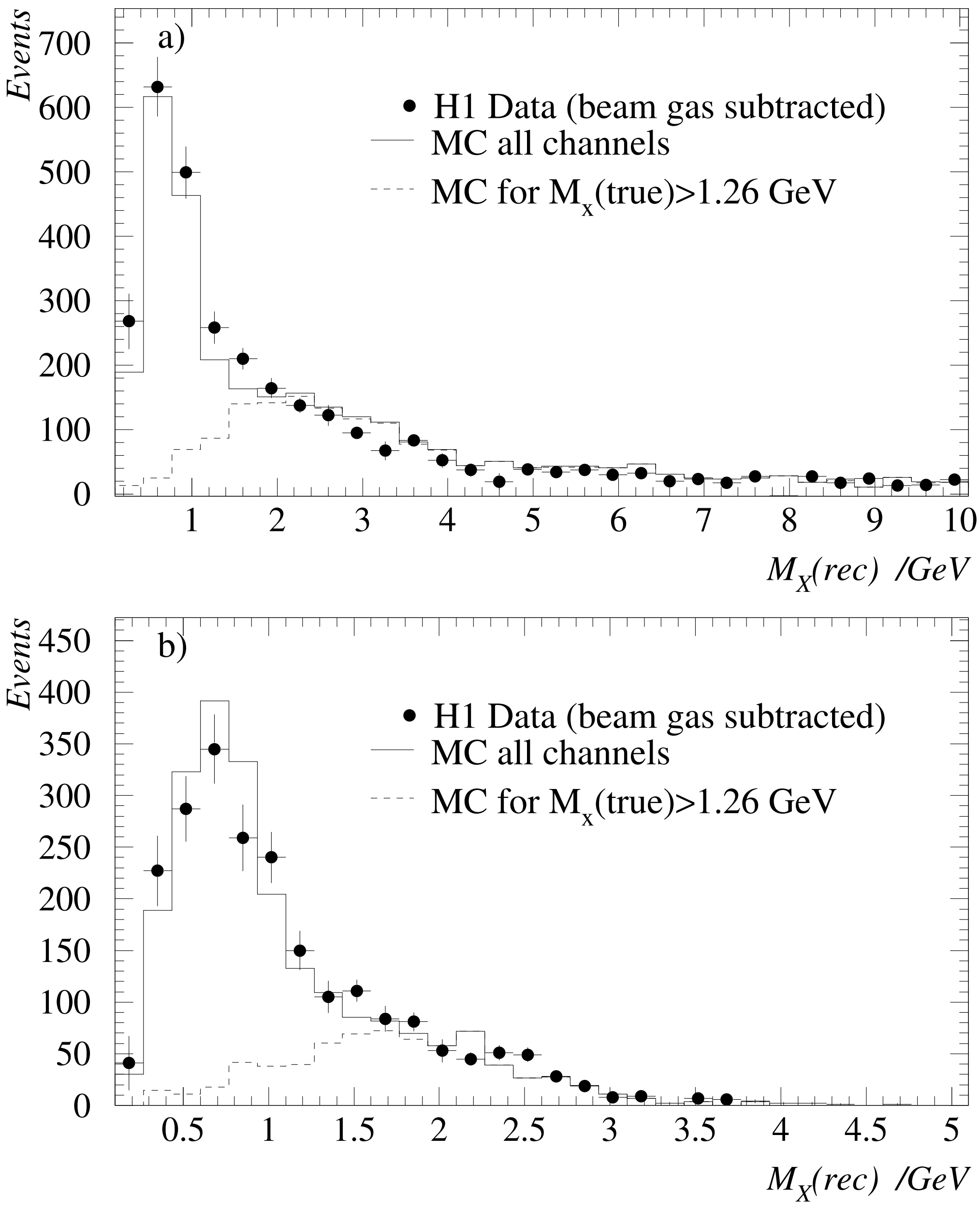

Figure 2: a) Reconstructed M_X distribution for the diffractive selection and b) for the elastic selection (without the $M_X < 1.26$ GeV cut) for the high $W_{\gamma p}$ analysis.

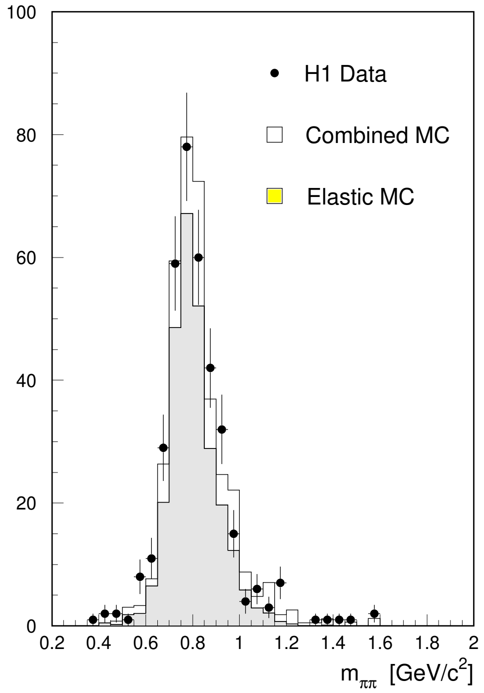

Figure 3: Final $m_{\pi\pi}$ distributions for data and MC events (MC histograms are normalized to data) for the low $W_{\gamma p}$ analysis. The MC mass shape shows good agreement with data.

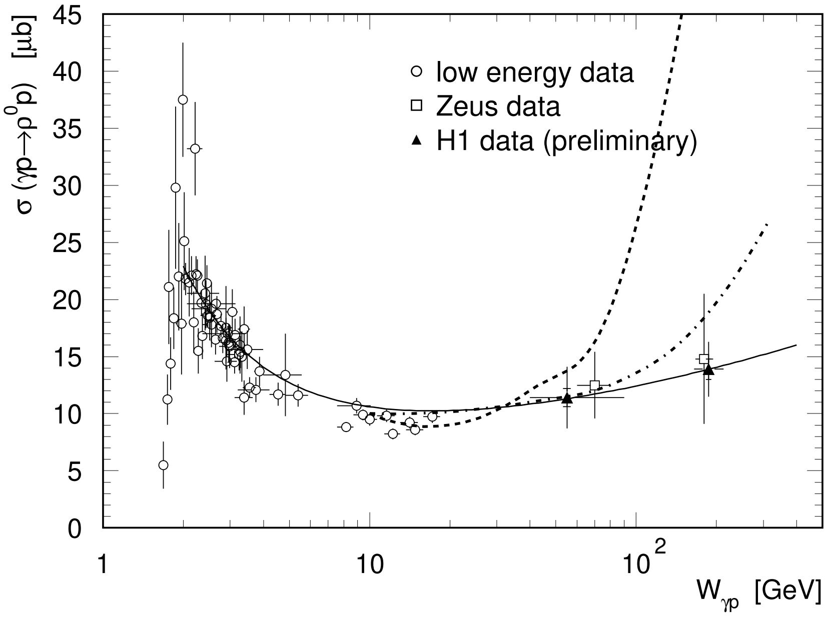

Figure 4: The elastic ρ^0 cross section, $\sigma(\gamma p \to \rho^0 p)$, versus $W_{\gamma p}$ for H1 and previous measurements. Also shown are theoretical predictions based on the additive quark model and VMD (solid curve), mini-jets with DG and $p_t^2 = 4$ (GeV/c)^2 (dot-dashed curve), and mini-jets with LAC1 and $p_t^2 = 4$ (GeV/c)^2 (dashed curve).

H1 preliminary

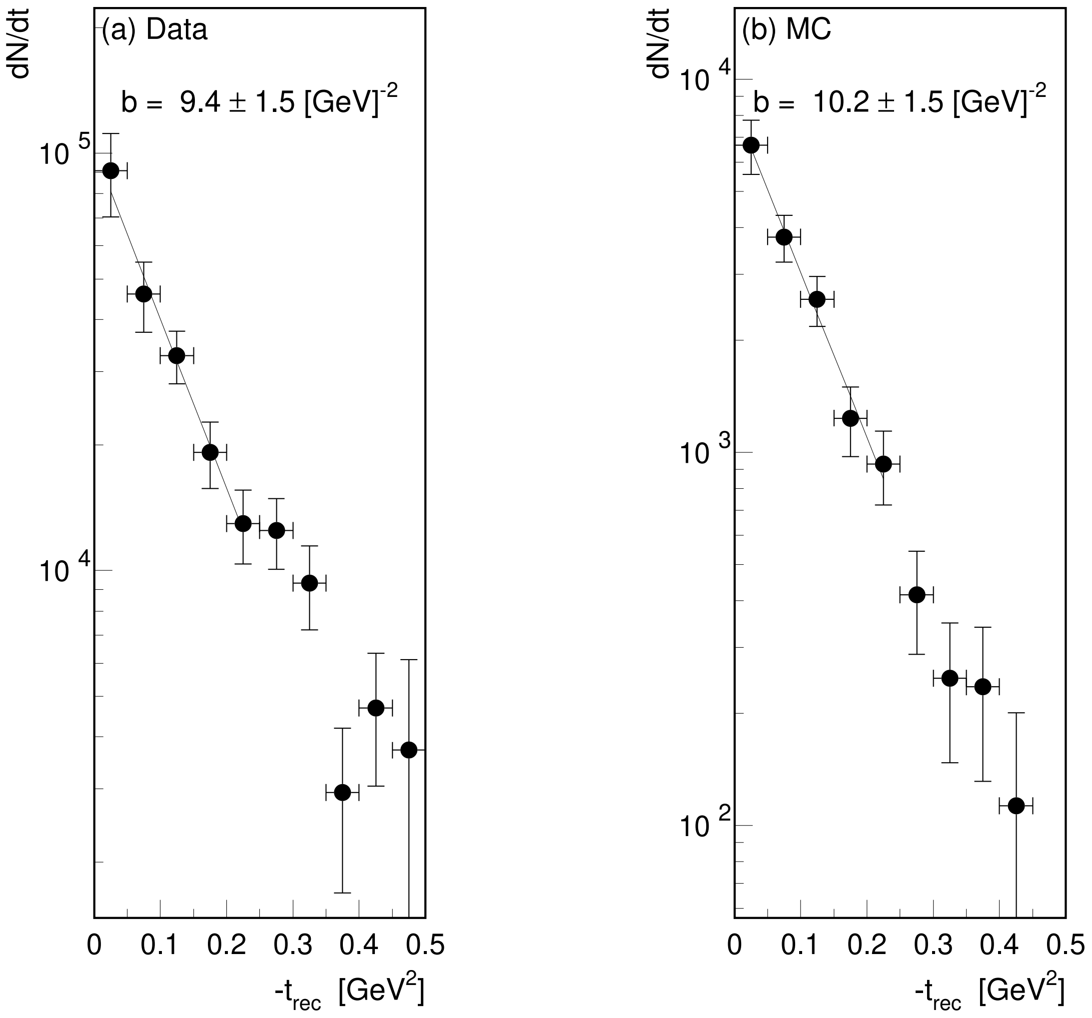

Figure 5: Final t distributions for: (a) data, after p-gas and inelastic background subtractions and acceptance correction; (b) combined MC histogram after inelastic subtraction and acceptance correction. The final histograms are fit with the function $dN/dt = a\,e^{bt}$ (statistical and systematic errors are summed in quadrature).

H1 preliminary

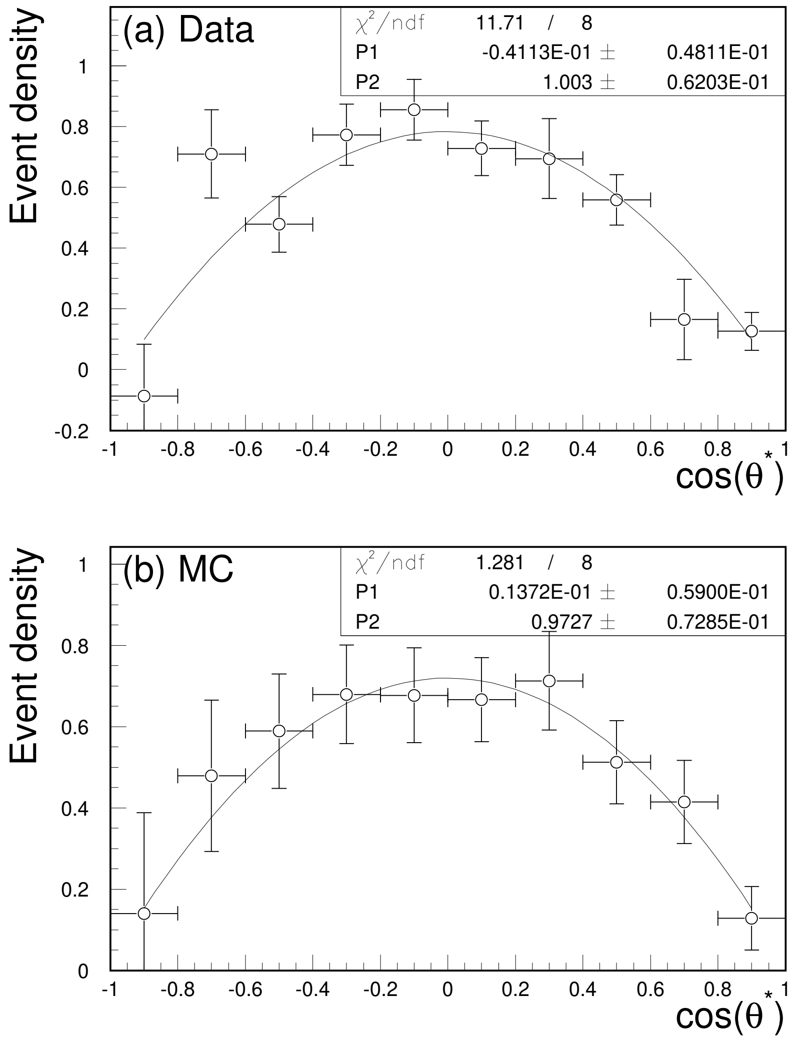

Figure 6: The final $\cos\theta^*$ density distributions for: (a) data (after beam-gas and inelastic subtractions and acceptance correction), and (b) combined MC distribution (after inelastic subtraction and acceptance correction). The two final plots have been fit with the $W(\theta^*)$ function (Eq. 21).

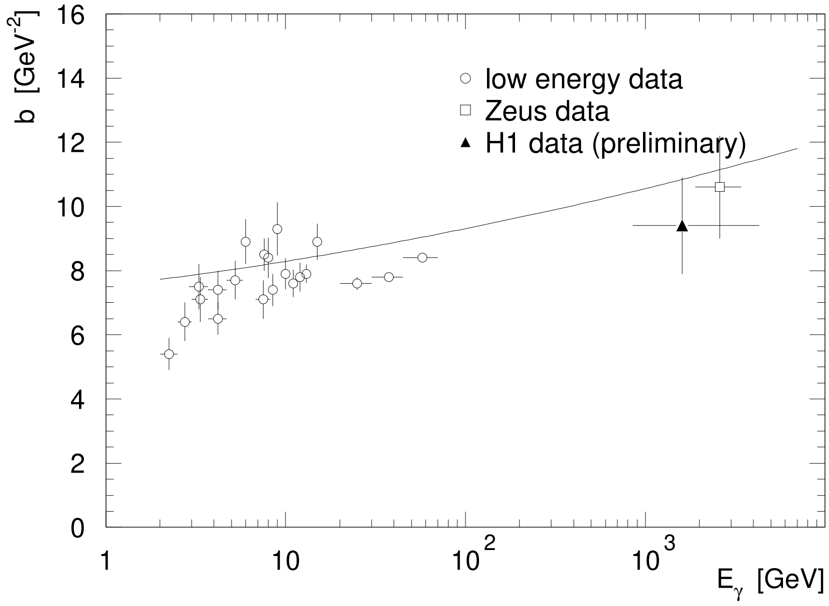

Figure 7: Determinations of the exponential slope parameter, b, as a function of E_γ, in the rest frame of the proton. The curve is a prediction based on pomeron exchange [5].